Aryl amination using ligand-free Ni(II) salts and photoredox catalysis

ORGANIC CHEMISTRY

Aryl amination using ligand-free Ni(II) salts and photoredox catalysis

Emily B. Corcoran,[1] Michael T. Pirnot,[2] Shishi Lin,[3] Spencer D. Dreher,[3] Daniel A. DiRocco,[3] Ian W. Davies,[3] Stephen L. Buchwald,[2]* David W. C. MacMillan[1]*

Over the past two decades, there have been major developments in transition metal–catalyzed aminations of aryl halides to form anilines, a common structure found in drug agents, natural product isolates, and fine chemicals. Many of these approaches have enabled highly efficient and selective coupling through the design of specialized ligands, which facilitate reductive elimination from a destabilized metal center. We postulated that a general and complementary method for carbon–nitrogen bond formation could be developed through the destabilization of a metal amido complex via photoredox catalysis, thus providing an alternative approach to the use of structurally complex ligand systems. Here, we report the development of a distinct mechanistic paradigm for aryl amination using ligand-free nickel(II) salts, in which facile reductive elimination from the nickel metal center is induced via a photoredox-catalyzed electron-transfer event.

Transition metal–catalyzed cross-coupling reactions are fundamental methods for constructing complex molecular architectures. Key among these reactions has been the formation of C–N bonds to access anilines, a common structure found in medicinal agents and other complex molecules, through the coupling of amines with aryl halides or pseudohalides (*1*–*6*). Over the past two decades, multiple generations of ligands have been designed that have elevated palladium-catalyzed aryl amination to an essential transformation with both predictable reactivity and practical importance. The ligand frameworks that have been developed for palladium catalysis often employ a few key design elements (i.e., sterically encumbered architecture, hemilabile coordinating groups, electronically tuned substituents) to enact high catalytic efficiency (*7*). One essential feature in ligand design is the capacity for destabilization of the Pd(II) amido complex, which induces reductive elimination resulting in C–N bond formation (*8*–*10*).

The broad success of ligated-palladium catalysis has hinged on the ability to selectively design, synthesize, and implement ligand classes to enable specific coupling reactions in high levels of efficiency and selectivity. Inspired by the effectiveness of structurally diverse ligand systems on palladium reductive elimination, we recognized that a general and complementary approach for productive C–N bond formation could be developed through an alternative mechanistic approach. In particular, we envisioned that the destabilization of a metal amido species could occur through an electron transfer pathway via photoredox catalysis, thus inducing facile C–N bond formation analogous to the role of ligand in traditional palladium couplings (Fig. 1).

We proposed that nickel could be an ideal transition metal for this catalytic platform because of its known proclivity to participate in one-electron processes (*11*–*13*). Furthermore, this ligand-free mechanism could potentially broaden the applicability of nickel catalysis in aryl amination (*14*–*18*), a system that is often plagued with the use of harsh reductants and air-sensitive Ni(0) complexes. Nickel(II) amido complexes, as detailed by Hillhouse and others, tend not to undergo reductive elimination at ambient temperature (*19*–*21*). Computations suggest that C–N reductive elimination from Ni(II) alkyl amido complexes is thermodynamically disfavored, in contrast to the exothermic reductive elimination from analogous Pd(II) alkyl amido complexes (*22*). Exposure of Ni(II) amido complexes to various oxidants results in facile reductive elimination, presumably through single-electron oxidation of the Ni(II) amido complex to the respective Ni(III) complex, lending support to our design strategy (*19*, *20*).

In recent years, the merging of photoredox catalysis with nickel catalysis has enabled both C–O (*23*) and C–S (*24*, *25*) bond formation through the generation of reactive radical intermediates and/or the single-electron modulation of nickel oxidation states (*26*, *27*). The feasibility of these reactions arises from the capacity of photocatalysts to act as both strong single-electron oxidants and reductants upon irradiation with visible light (*28*). Critical to the success of our design plan, the photoredox catalyst would be involved in two key aspects of our postulated mechanism: (i) reduction of a Ni(II) salt to the active Ni(0) catalyst through the use of a mild sacrificial reductant and (ii) electron transfer to destabilize the Ni(II) amido complex toward reductive elimination in the absence of an exogenous ligand.

In our proposed mechanism (Fig. 2), irradiation of heteroleptic Ir(III) photocatalyst Ir[dF(CF)$_3$ppy]$_2$(dtbbpy)PF$_6$ [dF(CF$_3$)ppy = 2-(2,4-difluorophenyl)-5-(trifluoromethyl)pyridine; dtbbpy = 4,4′-di-*tert*-butyl-2,2′-bipyridine] (**1**) with visible light would produce long-lived triplet photoexcited state *Ir^{III} **2** (τ = 2.3 μs) (*29*). Concomitantly, Ni(0) complex **3** would oxidatively insert into bromoarene **4** to yield the corresponding Ni(II) aryl bromide complex **5**. The Ni(II) complex would then undergo ligand exchange and subsequent deprotonation to arrive at Ni(II)-aryl amido complex **6**. This Ni(II) complex could then participate in a single-electron transfer (SET) event with the photoexcited *Ir^{III} catalyst ($E_{1/2}^{red}$ [*Ir^{III}/Ir^{II}] = + 1.21 V versus saturated calomel electrode (SCE) in CH$_3$CN) to afford Ni(III) complex **7** and the reduced Ir(II) photocatalyst (**8**) (*29*). Reductive elimination of the resultant Ni(III) complex would yield Ni(I) bromide species **9** and desired aniline product **10**. Both the photoredox and nickel catalytic cycles are closed upon a SET event between Ni(I)Br species **9** and Ir(II) ($E_{1/2}^{red}$ [Ir^{III}/Ir^{II}] = −1.37 V versus SCE in CH$_3$CN) in which Ni(0) catalyst **3** and ground state Ir(III) catalyst **1** are regenerated simultaneously (*29*). The homogeneous nickel species is presumably coordinated to solvent, base, and/or amine throughout the process (denoted as L$_n$ in Fig. 2), but would not require a designed ligand for efficient reactivity.

With this mechanistic hypothesis in hand, we first examined the proposed cross-coupling reaction with 4-bromobenzotrifluoride, pyrrolidine, Ni(II) bromide glyme, and a variety of ligands, bases, and solvents (see supplementary materials for details). The employment of photocatalyst **1**, 1,4-diazobicyclo[2.2.2] octane (DABCO) as a base and di-*tert*-butyl-2,2′-bipyridine as a supporting ligand provided the respective aniline product **10** in 72% yield in the presence of blue light. Control experiments established the importance of both nickel and photocatalyst, as no formation of the desired cross-coupled product was observed in the absence of either nickel, photocatalyst, or light. We sought to investigate the effectiveness of this protocol in the absence of ligand to confirm our initial mechanistic hypothesis. The cross-coupling reaction proceeded with enhanced reactivity in the absence of di-*tert*-butyl-2,2′-bipyridine, delivering the desired aniline product in 96% yield. This result supports our proposed mechanistic pathway in Fig. 2 and the capacity of visible light and a photocatalyst to initiate reductive elimination in the absence of ligand.

With the optimal conditions in hand, we sought to demonstrate the generality of this ligand-free amination. As highlighted in Fig. 3, a wide variety of functional groups were tolerated on the amine coupling partner, including protected nitrogen atoms, trifluoromethyl groups, alcohols, alkenes, and sulfonamides (**11** to **15**, 72 to 77% yield). The high efficiency of the photoredox catalytic cycle is evidenced by the low photocatalyst loadings [≤0.02 mole percent (mol %)] required to effect the desired cross-coupling reactions. Monofluorinated amines (**16**) coupled cleanly under these conditions in 81% yield. Coupling of amine

[1]Merck Center for Catalysis at Princeton University, Princeton, NJ 08544, USA. [2]Department of Chemistry, Massachusetts Institute of Technology, Cambridge, MA 02139, USA. [3]Department of Process Chemistry, Merck Research Laboratories, Rahway, NJ 07065, USA.
*Corresponding author. Email: dmacmill@princeton.edu (D.W.C.M); sbuchwal@mit.edu (S.L.B.)

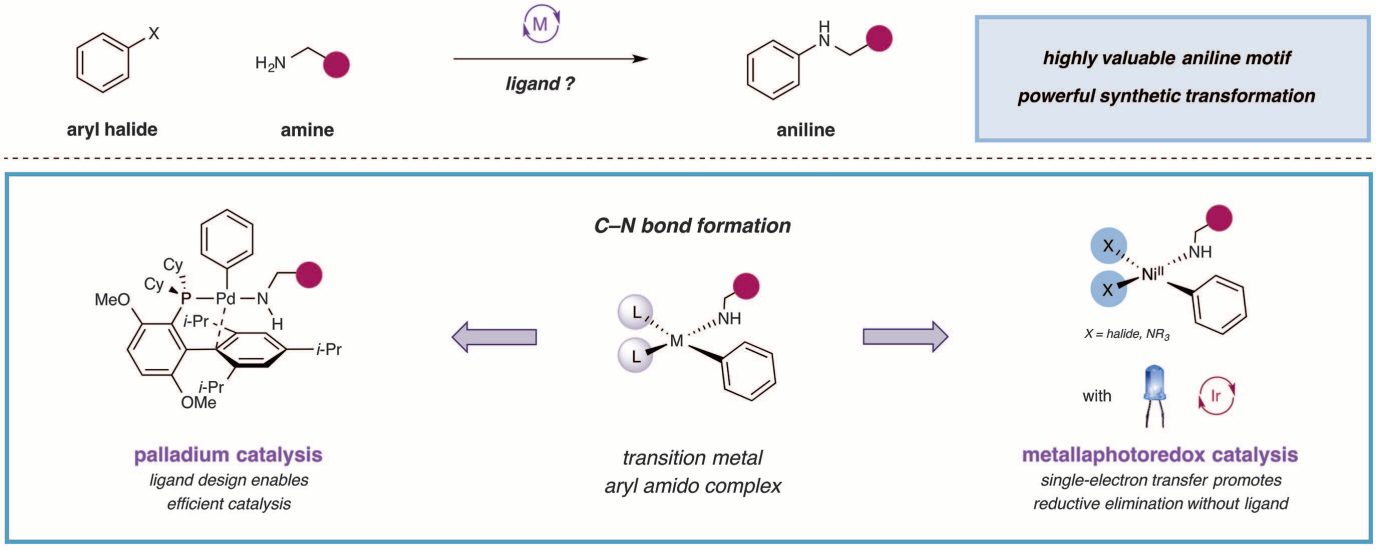

Fig. 1. Proposed approach to C–N cross-coupling—promotion of reductive elimination via single-electron transfer.

hydrogen chloride salts was accomplished in good yield by using MTBD (7-methyl-1,5,7-diazabicyclo-[4.4.0]deca-5-ene) as the base (**16** and **17**, 81 and 70% yield); although the expense of MTBD often limits its practicality, synthetically useful yields were also obtained with DABCO in most cases (see supplementary materials for details). Chemoselective *N*-arylation in the presence of alcohols was also achieved, as no C–O coupling was observed (**13**, 76% yield, single regioisomer).

We found that α-substitution on the amine partner was tolerated in moderate yields (**20** and **22**, 60 and 78% yield, respectively), but hindered amines, e.g., *tert*-butylamine, did not productively couple. Although nucleophilic amines, such as pyrrolidine and morpholine, coupled in good efficiencies (**10** and **22**, 96 and 91% yield, respectively) at ambient temperature after only a few hours, less nucleophilic substrates, such as trifluoroethylamine (**12**, 77% yield), allylamine (**14**, 76% yield), and furfurylamine (**23**, 90% yield), required longer reaction times (>24 hours). Amines lacking α-hydrogens failed to react under these reaction conditions. We hypothesized that an initial β-hydride elimination event is a prerequisite for accessing the active Ni(0) catalyst in this reaction. Indeed, the addition of a substoichiometric amount of amine possessing α-hydrogens, such as pyrrolidine, to the reaction resulted in good yields (72 and 84% yield) of cross-coupled products **15** and **24**, respectively, with less than 10% of the pyrrolidine-coupled product being observed. For a number of substrates, product formation was observed in high yield with $Ru(bpy)_3(PF_6)_2$ as the photocatalyst (see fig. S8). In cases where the yield is lower, protodehalogenation, along with trace phenol, aryl ether, or aryl chloride formation, can account for the mass balance of the reaction.

A variety of aryl bromides containing diverse functional groups, such as nitriles, amides, trifluoromethyl groups, halides, esters, and sulfonamides, performed well under the reaction conditions (**25** to **31**, 70 to 93% yield), with substitution at the ortho position being tolerated (**26** and **32**, 83 and 73% yield, respectively) (Fig. 3). Six-membered heteroaromatic substrates were effectively coupled in good yields (**27** and **33** to **35**, 71 to 91% yield). Unfortunately, a series of aryl bromides, e.g., select heterocycles and a 2,6-disubstituted arene, failed to couple under the current reaction conditions (see fig. S8). For electron-rich arenes (**32** and **36**), lowering the photocatalyst loading (0.002 mol %) increased reaction efficiency and inhibited competitive protodehalogenation, as did the use of MTBD as base. Additionally, the initial evaluation of this C–N

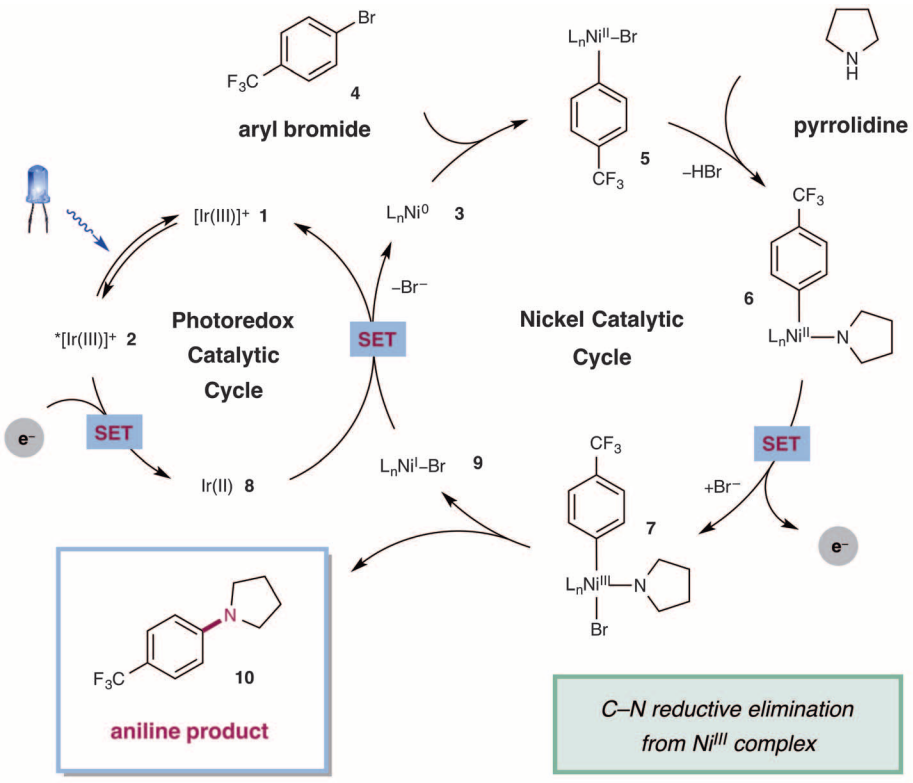

Fig. 2. Proposed mechanism for the metallaphotoredox-catalyzed amination reaction. L, DABCO or amine; SET, single-electron transfer.

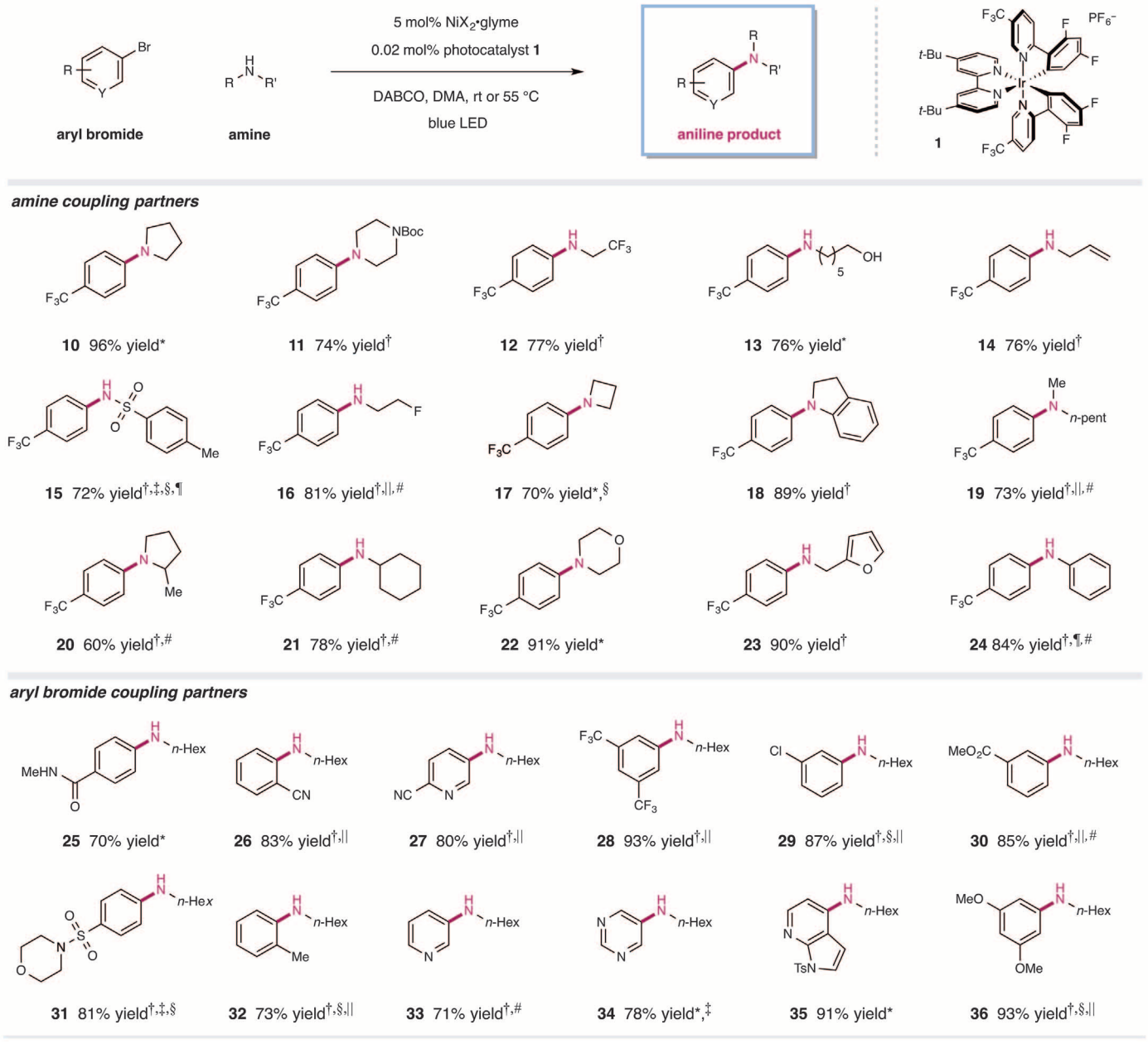

Fig. 3. Metallaphotoredox-catalyzed amination: amine and arene scope. For each entry number (in bold), data are reported as percent isolated yield. R: H, alkyl, or aryl substrate; Y: C, CH, or N; X: Cl or Br; DABCO: 1,4-diazabicyclo[2.2.2]octane; DMA, *N*,*N*-dimethylacetamide; rt, room temperature; LED: light-emitting diode; Me: methyl; *n*-pent: *n*-pentyl; Boc: *tert*-butoxycarbonyl. *Run at ambient temperature. †Reaction heated to 55°C. ‡DMSO (dimethyl sulfoxide) used as solvent. §MTBD (7-methyl-1,5,7-triazabicyclo[4.4.0]dec-5-ene) used as base. ‖0.002 mol % **1** used. ¶10 mol % pyrrolidine included. #See supplementary materials for details.

cross-coupling platform in flow chemistry has shown high efficiency in decreased reaction times (see supplementary materials).

To investigate the role of the photocatalyst in switching on nickel-catalyzed aryl amination, we used $Ni(cod)_2$. In the absence of light, the formation of aniline **10** was severely diminished (10% yield), whereas standard reaction conditions yielded **10** in 91% yield. This result supports our hypothesis that the cross-coupling is light-mediated and the effect of the photoredox catalyst is not limited to the reduction of a Ni(II) salt to the active Ni(0) species.

Lastly, this C–N cross-coupling platform was evaluated in a high-throughput fashion with a microscale informer plate as developed by Merck laboratories. A chemistry informer library of 18 complex, druglike aryl halides was subjected to Ni-photoredox–based amination conditions with piperidine. Notably, 78% of substrates underwent successful cross-coupling and provided "reaction hits" that were suitable for optimization (Fig. 4) (*30*). Benchmarked against other protocols that have been evaluated with this informer series, this study represents one of the most successful (*31*) generic catalysis platforms for aryl amination that has been evaluated within Merck. On the basis of these results, we are confident that this complementary method will find broad applicability in the synthesis of structurally diverse, druglike compounds.

Through the merger of photoredox and nickel catalysis, challenging C–N reductive elimination can be switched on through the use of visible light and a photocatalyst via the intermediacy of a Ni(III) oxidation state (*32*–*34*). This strategy represents a complementary approach to traditional ligated-palladium catalysis through the use of a distinct mechanistic pathway for reductive

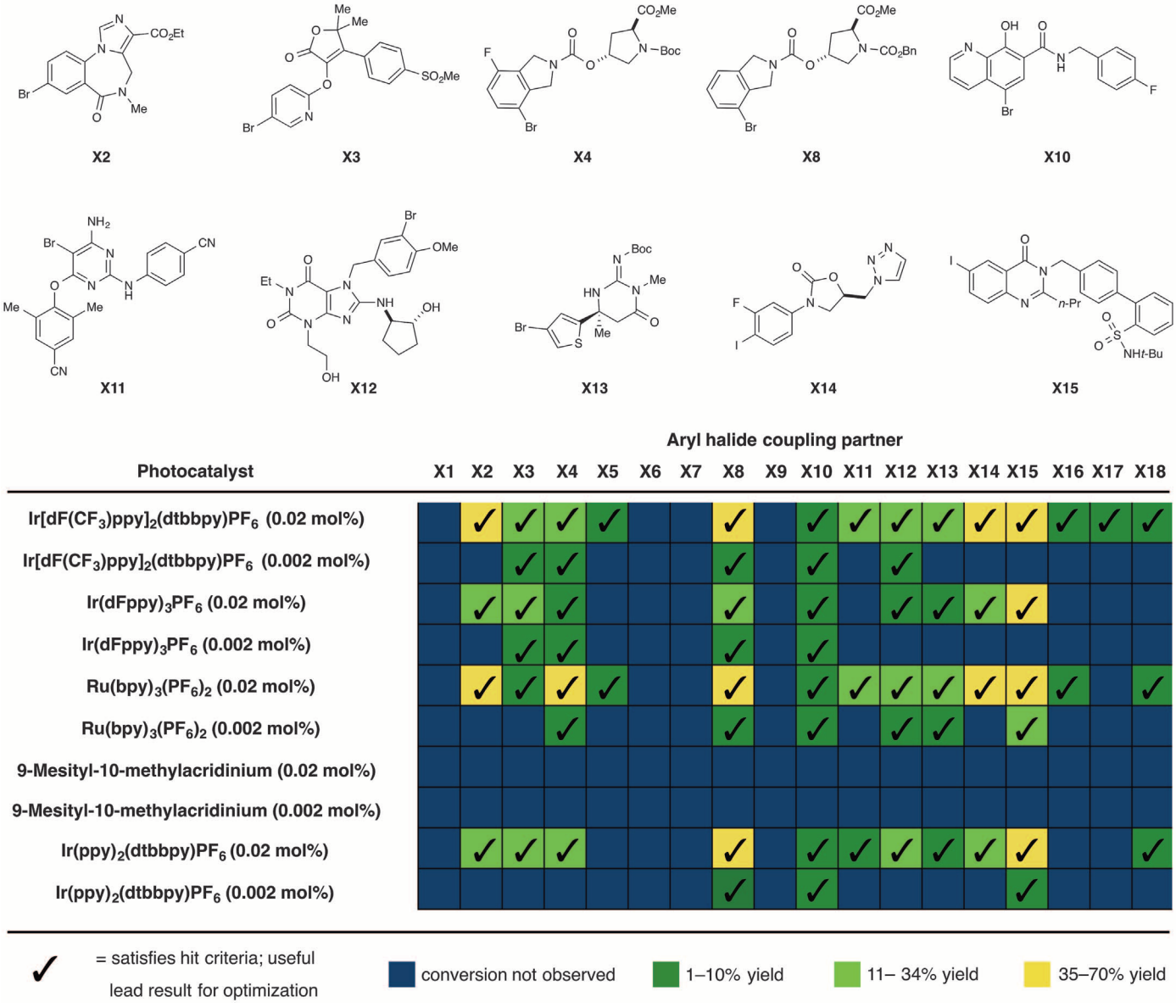

Fig. 4. High-throughput metallaphotoredox-catalyzed aryl amination with a chemistry informer library. For each compound numbered in bold, the cross-coupling was performed with piperidine using DABCO as a base. Ac, acetyl; Bn, benzyl; Boc, *tert*-butoxycarbonyl; Et, ethyl; Me, methyl; *n*-Pr, *n*-propyl; *t*-Bu, *tert*-butyl. Conversion was quantified by ultrapressure liquid chromatography/mass spectrometry (UPLC/MS) using an internal standard. See supplementary materials for exact yields and conditions.

elimination, which will likely be broadly applicable across a range of substrate classes.

REFERENCES AND NOTES

1. F. Ullmann, *Chem. Ber.* **36**, 2382–2384 (1903).
2. I. Goldberg, *Chem. Ber.* **39**, 1691–1692 (1906).
3. M. Kosugi, M. Kameyama, T. Migita, *Chem. Lett.* **12**, 927–928 (1983).
4. M. S. Driver, J. F. Hartwig, *J. Am. Chem. Soc.* **118**, 7217–7218 (1996).
5. D. Chan, *Tetrahedron Lett.* **37**, 9013–9016 (1996).
6. A. S. Guram, S. L. Buchwald, *J. Am. Chem. Soc.* **116**, 7901–7902 (1994).
7. D. S. Surry, S. L. Buchwald, *Chem. Sci.* **2**, 27–50 (2011).
8. B. P. Fors, D. A. Watson, M. R. Biscoe, S. L. Buchwald, *J. Am. Chem. Soc.* **130**, 13552–13554 (2008).
9. J. F. Hartwig, *Synlett* **1997**, 329–340 (1997).
10. A. T. Brusoe, J. F. Hartwig, *J. Am. Chem. Soc.* **137**, 8460–8468 (2015).
11. T. T. Tsou, J. K. Kochi, *J. Am. Chem. Soc.* **101**, 6319–6332 (1979).
12. The use of ligated nickel and photoredox catalysis for C–N bond formation has been reported (*13*).
13. S. Z. Tasker, T. F. Jamison, *J. Am. Chem. Soc.* **137**, 9531–9534 (2015).
14. J. P. Wolfe, S. L. Buchwald, *J. Am. Chem. Soc.* **119**, 6054–6058 (1997).
15. C.-Y. Gao, L.-M. Yang, *J. Org. Chem.* **73**, 1624–1627 (2008).
16. N. H. Park, G. Teverovskiy, S. L. Buchwald, *Org. Lett.* **16**, 220–223 (2014).
17. S. Ge, R. A. Green, J. F. Hartwig, *J. Am. Chem. Soc.* **136**, 1617–1627 (2014).
18. T. Shimasahi, M. Tobisu, N. Chatani, *Angew. Chem. Int. Ed.* **49**, 2929 (2010).
19. K. Koo, G. L. Hillhouse, *Organometallics* **14**, 4421–4423 (1995).
20. B. L. Lin, C. R. Clough, G. L. Hillhouse, *J. Am. Chem. Soc.* **124**, 2890–2891 (2002).
21. L. Ilies, T. Matsubara, E. Nakamura, *Org. Lett.* **14**, 5570–5573 (2012).
22. S. A. Macgregor, G. W. Neave, C. Smith, *Faraday Discuss.* **124**, 111–127, discussion 145–153, 453–455 (2003).
23. J. A. Terrett, J. D. Cuthbertson, V. W. Shurtleff, D. W. C. MacMillan, *Nature* **524**, 330–334 (2015).
24. M. S. Oderinde, M. Frenette, D. W. Robbins, B. Aquila, J. W. Johannes, *J. Am. Chem. Soc.* **138**, 1760–1763 (2016).
25. M. Jouffroy, C. B. Kelly, G. A. Molander, *Org. Lett.* **18**, 876–879 (2016).
26. J. C. Tellis, D. N. Primer, G. A. Molander, *Science* **345**, 433–436 (2014).
27. Z. Zuo *et al.*, *Science* **345**, 437–440 (2014).
28. C. K. Prier, D. A. Rankic, D. W. C. MacMillan, *Chem. Rev.* **113**, 5322–5363 (2013).
29. M. S. Lowry *et al.*, *Chem. Mater.* **17**, 5712–5719 (2005).

30. Previous studies leveraging high-throughput experimentation at Merck validated 5% yield as a good screening hit and 20% yield as a robust hit.
31. P. S. Kutchukian *et al*., *Chem. Sci. (Camb.)* **7**, 2604–2613 (2016).
32. $NiCl_2$ has been reported as a heterogeneous catalyst for the *N*-arylation of aryl iodides under microwave conditions in the absence of an exogenous ligand (*33*).
33. A. K. Gupta, G. T. Rao, K. N. Singh, *Tetrahedron Lett.* **53**, 2218–2221 (2012).
34. Although we favor the mechanism outlined in Fig. 2, we cannot rule out the possibility of energy transfer or direct excitation of Ni(II) in the presence of visible light.

ACKNOWLEDGMENTS

Research reported in this publication was supported by the NIH under award numbers GM58160 and RO1-GM078201-05. The content is solely the responsibility of the authors and does not necessarily represent the official views of the NIH. M.T.P. thanks the NIH for a postdoctoral fellowship (GM113311).

SUPPLEMENTARY MATERIALS

www.sciencemag.org/content/353/6296/279/suppl/DC1
Materials and Methods
Supplementary Text
Figs. S1 to S12
References (*35*–*48*)
NMR Spectra

30 April 2016; accepted 3 June 2016
Published online 23 June 2016
10.1126/science.aag0209

GLACIERS

Ocean forcing of glacier retreat in the western Antarctic Peninsula

A. J. Cook,[1,2]* P. R. Holland,[3] M. P. Meredith,[3] T. Murray,[1] A. Luckman,[1] D. G. Vaughan[3]

In recent decades, hundreds of glaciers draining the Antarctic Peninsula (63° to 70°S) have undergone systematic and progressive change. These changes are widely attributed to rapid increases in regional surface air temperature, but it is now clear that this cannot be the sole driver. Here, we identify a strong correspondence between mid-depth ocean temperatures and glacier-front changes along the ~1000-kilometer western coastline. In the south, glaciers that terminate in warm Circumpolar Deep Water have undergone considerable retreat, whereas those in the far northwest, which terminate in cooler waters, have not. Furthermore, a mid-ocean warming since the 1990s in the south is coincident with widespread acceleration of glacier retreat. We conclude that changes in ocean-induced melting are the primary cause of retreat for glaciers in this region.

The Antarctic Peninsula (AP) glaciers north of 70°S have the potential to raise sea level by 69 ± 5 mm (*1*), so any imbalance in their mass budget is of global importance. The region has undergone rapid warming in the latter half of the 20th century (*2*), and it is widely accepted that this has had a substantial impact on the ice sheet (*3*–*6*). The established theory that retreat of floating ice shelves is linked to a southerly migration of an atmospheric thermal limit (*7*) might also be considered likely to apply to retreat of marine-terminating glacier fronts. Indeed, the most significant glacier area loss over the past few decades has occurred in the northeast (*8*), which is north of the thermal limit and where the atmospheric temperature rise has been greatest.

Glaciers flowing westward from the AP plateau have, however, shown notable differences in frontal change over the same period. Overall ice loss has been greater in the south than the north, and glaciers in the northwest have remained stable (*8*). A previous study suggested that atmospheric warming may not be responsible for glacier change in this region because the migration from advance to retreat implied a warming more rapid than that observed (*9*). Indeed, spatial and temporal patterns of atmospheric forcings, including surface temperatures (*10*), melt duration (*4*), and precipitation (*11*), exhibit no clear relationship with the distinct north-south gradient of glacier-front changes along the west coast (*8*).

In the southwestern Bellingshausen Sea, rapid thinning of the ice shelves and their tributary glaciers has occurred during the past decade (*12*, *13*), and it has been proposed that this is caused by changes in upper-ocean heat content (*14*, *15*). The much larger ice loss from the West Antarctic Ice Sheet has also been linked to changes in heat content in the adjacent Amundsen Sea (*16*, *17*), which is similarly dominated by Circumpolar Deep Water (CDW) in its deeper layers. There, basal melting causes ice-shelf thinning, grounding-line retreat, and a loss of buttressing to the grounded ice inland. Variations in tidewater glacier termini are more complex, but several recent studies of Arctic glaciers have concluded that calving rates are strongly dependent on ocean temperatures [e.g., (*18*)]. Until now, the role of the ocean (as opposed to the atmosphere) as the dominant driver of glacier frontal retreat on the western AP has not been considered.

Although the oceans around Antarctica are notoriously data-sparse, the World Ocean Database 2013 (*19*) contains a sufficiently high spatial density of ocean temperature and salinity measurements to the west of the AP to enable regional mean temperature estimations (1945 to 2009) (*20*). When considered alongside observed changes in the glacier fronts (Fig. 1), a strong spatial correlation between the distribution of retreating glaciers and the pattern of mean ocean temperature over this period is revealed. Nearly all the glaciers south of Brabant and Anvers islands (~65°S), which discharge into warm ocean regions dominated by CDW, have suffered retreat. In contrast, the more northerly glaciers, which discharge into the cooler Bransfield Strait Water (BSW), experienced only small frontal changes indicative of relative stability over the 65 years for which observations are available. Furthermore, a southward increase in ice loss per glacier revealed in an earlier study (*8*) corresponds to a distinct and coherent spatial distribution in ocean temperatures (Fig. 2A). Ocean temperatures in this region are highly variable in the upper 100 m, but a pronounced north-south gradient becomes progressively more apparent at greater depth.

Partitioning the ocean adjacent to the AP into six regions of approximately equal area reveals three distinct oceanographic regimes (*21*, *22*) (Fig. 2, B and C). To the south and west, warm and saline CDW is prevalent across the Bellingshausen Sea shelf. This CDW is overlain by colder and fresher Winter Water (WW) and Antarctic Surface Water (AASW) formed by the interaction of CDW with the cryosphere and atmosphere. To the northeast, the Weddell Sea shelf contains cold and saline Shelf Water, which is heavily influenced by heat loss to the atmosphere and sea-ice production in the Weddell Sea. In the Bransfield Strait, northwest of the AP, the BSW is a mixture of Shelf Water and variants of CDW, again modified by air-sea-ice interaction. Crucially, these three water masses present very different thermal forcing to the glaciers abutting the ocean: the Shelf Water, BSW, and CDW average approximately 1°, 2°, and 4°C above the seawater freezing temperature, respectively (Fig. 2C). Glacier melting is expected to increase linearly or above-linearly with temperature above freezing, depending upon the geometry of the ice face and the presence of subglacial meltwater discharge (*23*, *24*).

The relationship between the ocean temperatures and glacier front change is also quantitatively robust (Fig. 3). Glaciers that have the warmest ocean temperatures near their fronts have retreated most significantly, and glaciers that are adjacent to the coolest water have remained stable or advanced. The relationship is strongly depth-dependent: Temperatures at and below 150-m depth display similar correlations,

[1]Department of Geography, Swansea University, Swansea, UK. [2]Department of Geography, Durham University, Durham, UK. [3]British Antarctic Survey, High Cross, Madingley Road, Cambridge, UK.
*Corresponding author. Email: alison.cook@durham.ac.uk

Aryl amination using ligand-free Ni(II) salts and photoredox catalysis

Emily B. Corcoran, Michael T. Pirnot, Shishi Lin, Spencer D. Dreher, Daniel A. DiRocco, Ian W. Davies, Stephen L. Buchwald and David W. C. MacMillan

Science **353** (6296), 279-283.
DOI: 10.1126/science.aag0209originally published online June 23, 2016

A light approach to C-N bond formation

The need to form C-N bonds arises frequently in drug discovery research. One versatile approach involves the attachment of the C and N fragments to a Pd catalyst. This approach needs a bulky ligand to "crowd" the fragments together off the metal center. Corcoran *et al.* present a complementary approach that uses Ni in place of Pd. Instead of the bulky ligand, they used a light-activated cocatalyst that strips an electron from the Ni to accelerate the bond formation. A screen involving elaborately substituted reagents confirmed the utility of this approach in cases that challenge the traditional Pd coupling.

Science, this issue p. 279